Bushra M. Ghdhaib
Sahar N. Rashid

Department of Physics,
College of Science,
University of Tikrit,
Tikrit, IRAQ

Characterization of Nickel and Nickel Oxide Nanoparticles Prepared by Laser Ablation Technique: Effect of Laser Wavelength and Energy

Pulsed laser ablation in liquids is a process that has many advantages over traditional methods used to prepare nanoparticles. A piece of pure, polished nickel metal was used to prepare nanoparticles using pulsed laser ablation technique in ethanol using Nd:YAG laser with three wavelengths (1064, 532, and 355nm) and three energies (50, 100, and 150mJ). This work focuses on evaluating the extent of the influence of some ablation parameters on the properties of prepared nanoparticles by characterizing them structurally and optically. The results showed the formation of both nickel nanoparticles and nickel oxide nanoparticles with spherical shapes and with an average diameter ranging between 11.35 and 76.6 nm. It was found that the oxidation rate increases when the shorter wavelength of the laser is used in the preparation. Absorbance increases with increasing laser energy, and the most appropriate wavelength and laser energy in preparation are 532nm and 150mJ. This technique has proven to be one of the easiest physical methods for preparing nanoparticles of metals and their oxides and is characterized by its speed and low cost.

Keywords: Laser ablation; Colloidal solutions; Nanoparticles; Nickel oxide
Received: 08 March 2024; **Revised:** 30 April 2024; **Accepted:** 07 May 2024

1. Introduction

One-step, top-down, easy, fast, economical, and environmentally friendly is, in short, the most important description of the pulsed laser ablation in liquid (PLAL) technique to prepare nanoparticles (NPs) [1-4]. One of the many advantages of this approach is the ability to control the shape, morphology, size, and properties of the produced NPs [5-7]. This control results from the control of various ablation parameters, such as laser energy, laser pulse width, repetition rate, wavelength, ablation time, and fluid height level above the target surface [8-11]. This technique depends on laser ablation, which has a high intensity to result in the interaction of the laser with the surface of the target material, thus producing a plasma plume immersed in the liquid. Special thermodynamic conditions arise when both pressure and temperature are high, which allows the production of NPs [11]. Figure (1) shows the mechanism of nanoparticle formation by laser ablation [12].

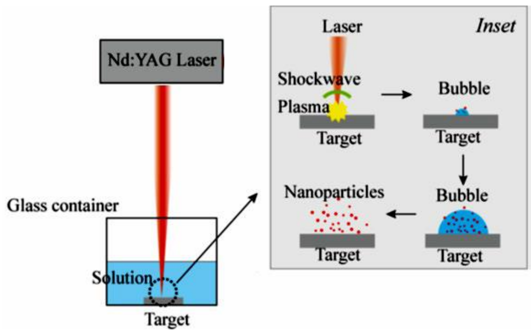

Fig. (1) Schematic diagram of PLAL process

Depending on the wavelength of the laser used, its energy works to oscillate the free electrons on the surface of the metal target collectively, where absorption and scattering occur. This mechanism is a result of the ability of metal nanoparticles to absorb visible light by creating a collective vibration of the conduction bands, which are in strong resonance with specific frequencies. This phenomenon is a unique feature of metallic NPs called surface plasmon resonance (SPR), which results in measurable changes in the NPs optically as the electromagnetic field in the surroundings is enhanced by plasmon excitation [5]. Among the many metal nanoparticles that are the subject of extensive research, nickel (Ni) NPs are distinguished for their wide applications resulting from their properties, the most important of which are extreme catalytic activity, superparamagnetic properties, and antibacterial effects [13-18]. In addition, nickel oxide NPs have received great attention in a variety of scientific fields because they have important physical, biological, and chemical properties [19-24].

This work aims to evaluate the effect of changing some laser parameters, namely energy, and wavelength, on the optical and structural properties of NPs prepared from a pure nickel piece using the pulsed laser ablation technique in a liquid medium, to enable control over the properties of the resulting nanoparticles.

2. Experimental Part

Nd:YAG laser, with wavelengths of 355, 532, and 1064 nm, energies of 50, 100, and 150 mJ, number of pulses of 500, and repetition rate of 3 Hz, was used to prepare three solutions of colloidal NPs in 3 ml of absolute ethanol utilizing a pure nickel metal piece with dimensions 10×10×1 mm, where the ethanol level was 1 cm high above the Ni target and the distance between the laser source and Ni target was 15 cm.

To evaluate the influence of energy and wavelength on the most important structural and optical characteristics of the prepared colloidal solutions containing the nanoparticles, the diagnosis of these properties was done using x-ray diffraction (XRD), the field-emission scanning electron microscopy (FE-SEM), the energy-dispersive x-ray spectroscopy (EDX), the Fourier-transform infrared (FTIR) spectroscopy, and UV-visible spectrophotometry. XRD was used to determine, in addition to the crystalline structure, the average sizes of the prepared nanoparticles using the Debye–Scherrer's equation [25]:

$$D = \frac{0.9\times\lambda}{\beta Cos\theta} \quad (1)$$

where λ is the wavelength of the x-ray (1.54Å), θ is the angle of diffraction, and β is the full-width at half maximum (FWHM) of the diffraction peaks using different laser fluencies. FE-SEM was used to determine the morphology and average diameter of the prepared NPs, EDX was used to calculate the proportions of the components of the colloidal solutions, FTIR spectroscopy was used to determine the compositions of the resulting colloidal solutions and the active groups in them, and UV-visible spectrophotometry was used to record the absorption spectra of the prepared NPs and to calculate the optical conductivity (σ) using the equation (2) [26], and the energy gap using the Tauc's equation (3) [27]

$$\sigma = \frac{\alpha nc}{4\pi} \quad (2)$$

$$\alpha h\upsilon = B(h\upsilon - E_g)^{\frac{1}{2}} \quad (3)$$

where α is the absorption coefficient, c is the velocity of light, n is the refractive index, B is a constant, h is the Planck's constant, υ is the photon frequency, and E_g is the energy gap

3. Results and Discussion

XRD patterns of nano-colloidal solutions prepared by laser ablation at the three wavelengths at the highest preparation energy in this work (150 mJ) show the formation of cubic-phase Ni NPs according to JCPDS card no. 00-001-1260, and NiO NPs with two dominant phases were also formed. They are cubic for nickel oxide nanoparticles (NiO NPs) according to JCPDS card no. 47-1049 and hexagonal for nickel trioxide nanoparticles (Ni_2O_3 NPs) according to JCPDS card no. 00-01-0481, as in Fig. (2). The appearance of oxides and other additional peaks is due to the interactions between the extracted nickel and the surrounding liquid, in addition to the difference in molecular pressures in the preparation space due to laser energy, where the preparation process took place in the air. Table (1) summarizes the results of XRD analysis and shows that the average sizes of NPs calculated using Eq. (1) are 27.6, 26.5, and 29.84 nm, for the samples prepared at wavelengths of 1064, 532, and 355 nm, respectively. It turns out that using the wavelength of 532 nm led to the production of NPs with a smaller average size, meaning that using a shorter wavelength (532 nm) caused an increase in laser flux, which in turn caused a decrease in the average size of the resulting NPs, as in [9]. Continuing to increase the laser energy flux using the shorter wavelength (355 nm) of the laser, led to the NPs aggregation, which led to an increase in their average sizes as a result of an increase in the ablation rate.

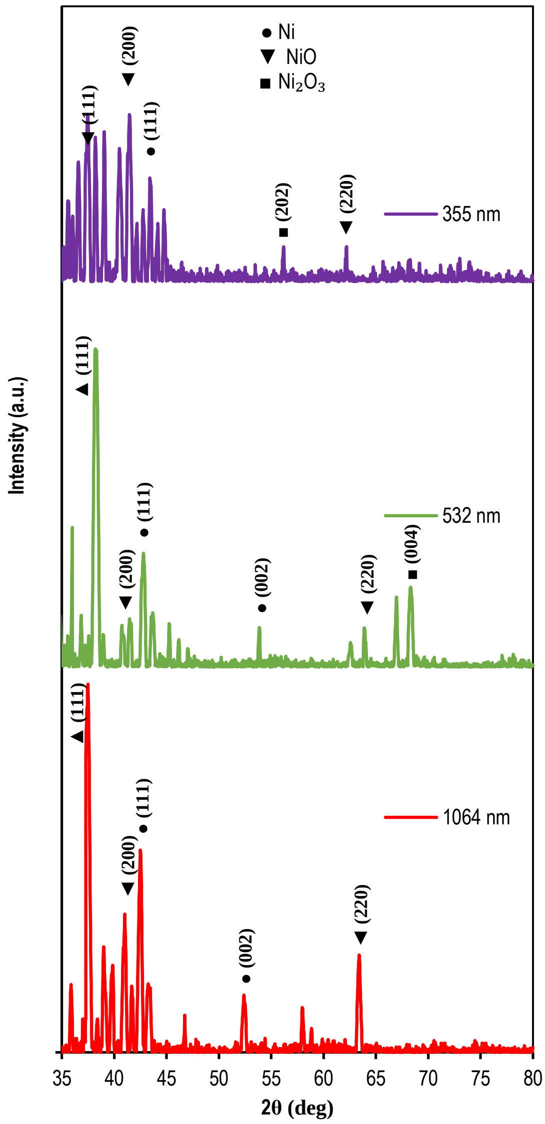

Fig. (2) XRD patterns of prepared NPs at 150 mJ

The FE-SEM analysis of nano-colloidal solutions prepared at the energy of 150 mJ, which is shown in figures (3), (4), and (5) using wavelengths of 1064, 532, and 355 nm, respectively, shows the average diameters and the morphology of the prepared samples, and at scales of 100 nm and 10 μm, where the average diameters of the prepared NPs are 76.6, 11.35, and 19.9 nm using wavelengths of 1064, 532, and 355 nm, respectively. The scale of 100 nm shows the average diameters of the prepared NPs, while the other scale (10 µm) shows its shape in addition to the resulting agglomerations, and this magnification image shows good contrast of the structure. This is consistent with what was stated in the results of the XRD analysis, where the average sizes of NPs were smaller when prepared using 532 nm of laser radiation.

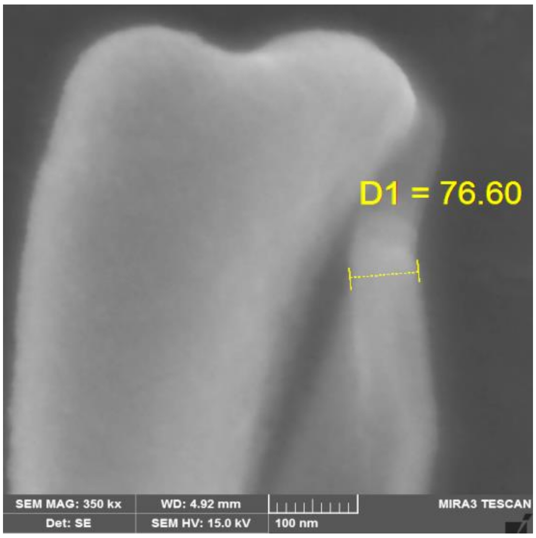

(a)

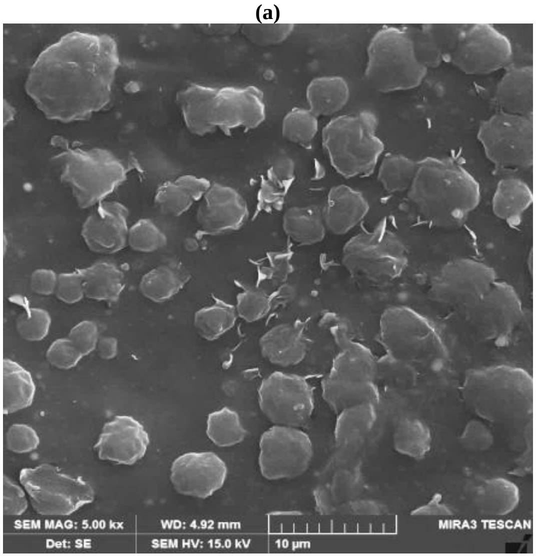

(b)

Fig. (3) FE-SEM images of prepared NPs using 1064nm with scale of (a) 100nm, (b) 10µm

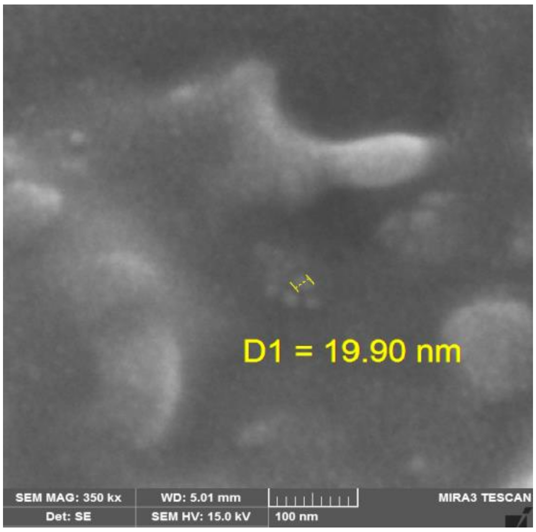

(a)

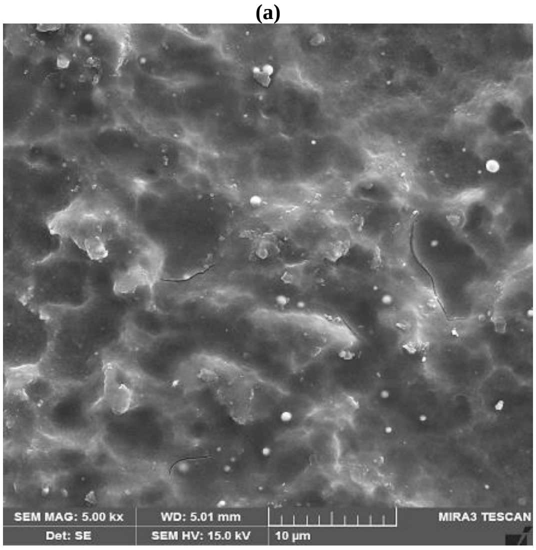

(b)

Fig. (4) FE-SEM images of prepared NPs using 532nm with scale of (a) 100nm, (b) 10µm

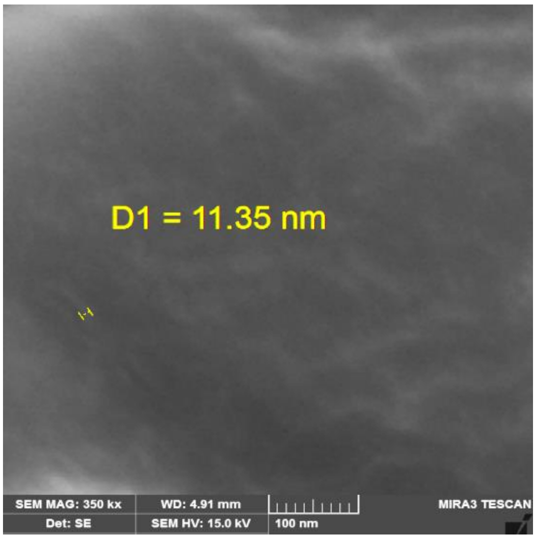

(a)

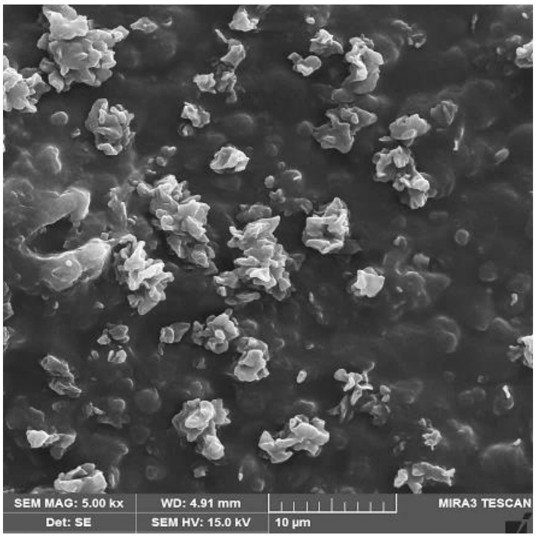

(b)

Fig. (5) FE-SEM images of prepared NPs using 355 nm with scale of (a) 100nm, (b) 10µm

The elemental compositions of the samples prepared using an energy of 150 mJ were analyzed. They showed an increase in oxidation rates consistent with what appeared in the results of XRD analysis, as in figures (6), (7) and (8), where the source of oxygen (O) in these figures is the oxidation resulting from the surrounding environment, as the ablation process did not take place in a vacuum, and it may result from the environment surrounding the EDX device itself, in addition to the fact that the preparation medium is ethanol which containing the oxygen element. The weight percentages, atomic percentages, and k-ratio of oxygen increased with laser fluence by decreasing the laser wavelength used to prepare the samples and were calculated based on the weight and atomic percentages and k-ratio of Ni as in table (2).

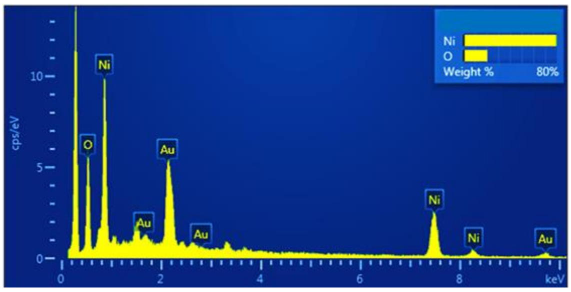

Fig. (6) EDX spectrum of NPs prepared using 1064 nm

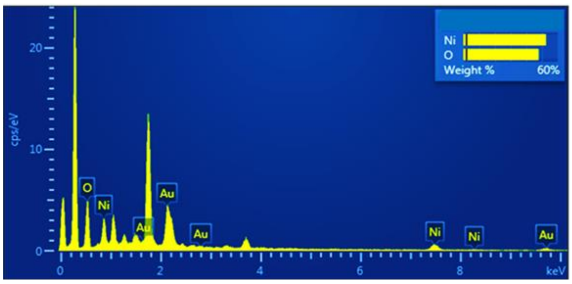

Fig. (7) EDX spectrum of NPs prepared using 532 nm

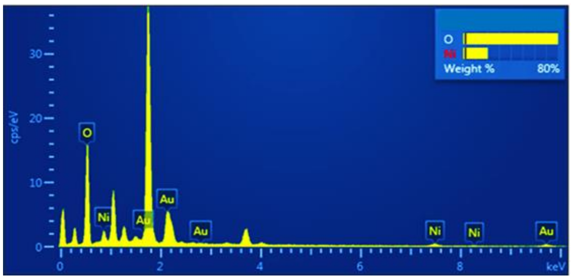

Fig. (8) EDX spectrum of NPs prepared using 355 nm

The results of FTIR measurements included an analysis of all samples prepared using wavelengths of 1064, 532, and 355 nm, as in figures (9), (10), and (11), respectively, from which the effective groups consisting of O-H, O-H-O, and C-O bonds are evident in all spectra representing samples prepared in ethanol. The occurrence of some slight shifts and differences in absorption intensity was noted as a result of the effect of laser parameters, and the effect of nickel NPs and its oxide, where the shapes show bending and stretching vibrations around 400 and 600 cm^{-1}, which are the result of Ni-O (which is the focus of this study). This result is consistent with [28] and [29].

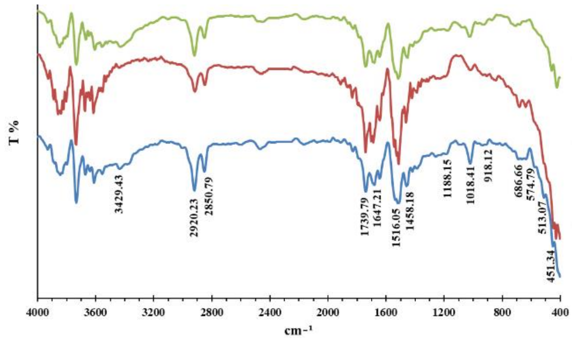

Fig. (9) FTIR spectrum of NPs prepared using 1064nm (Green 150mJ, Red 100mJ, Blue 50mJ)

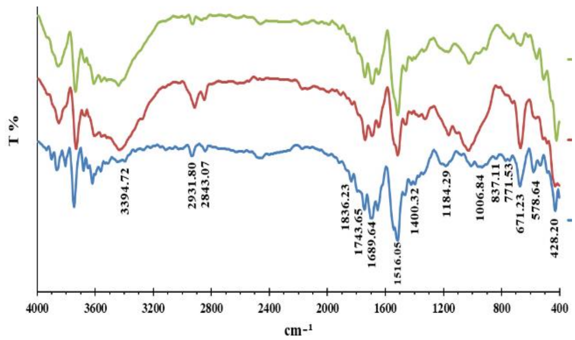

Fig. (10) FTIR spectrum of NPs prepared using 532nm (Green 150mJ, Red 100mJ, Blue 50mJ)

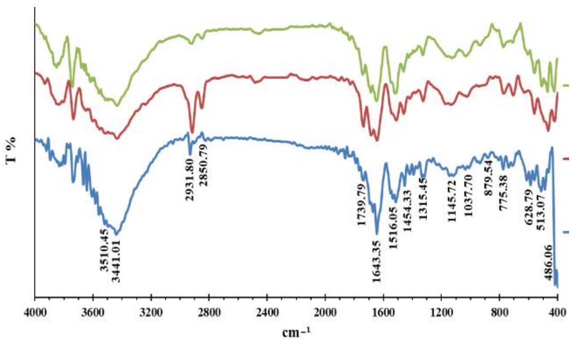

Fig. (11) FTIR spectrum of NPs prepared using 355nm (Green 150mJ, Red 100mJ, Blue 50mJ)

Figures (12), (13), and (14) represent the absorption and optical conductivity spectra, in addition to the energy gap, of the prepared NPs using wavelengths of 1064, 532, and 355 nm, respectively. These figures, in general, show that the absorbance increases with increasing laser energy for all wavelengths used, in addition to the broadening of the peak width. The appearance of these peaks representing SPR around the wavelength of 295 nm is attributed to the frequency of the incident light photons matching the frequency of the surface electrons of the NPs. This is attributed to the coloring of the resulting solution and growth in intensity with increasing laser fluence as a result of increasing the laser energy and thus increasing the concentration of NPs in the solution, which in turn means increasing the number of extracted NPs. This works to increase the absorbance as these NPs have the property of increasing the surface-to-volume ratio, so they are highly effective, and as a result, the absorbance increases. The results show that the optical conductivity of the prepared NPs peaks approximately in the SPR region, and its value is affected by changing the ablation parameters, as it increases with increasing preparation energy. Since the optical properties of materials, in general, depend on their structural properties, the optical energy gap of the prepared samples was calculated as a result of changing the composition of the samples, as the appearance of the metal oxide NPs detected in the XRD analysis of the prepared samples means the formation of an energy gap for them. Energy gap values were 3.9-3.89 eV, 3.42-3.38 eV, and 3.56-3.42 eV for NPs prepared using the wavelengths of 1064, 532, and 355 nm, respectively. It was observed that their values decrease when the laser energy is increased, that is, the conductivity of nanoparticles increased with the increase in their acquisition of the applied energy.

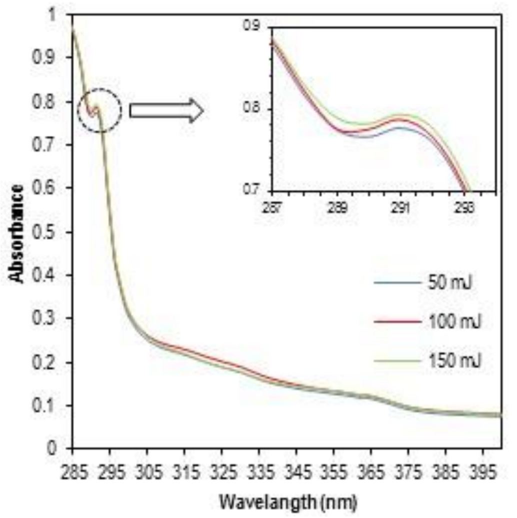

(a)

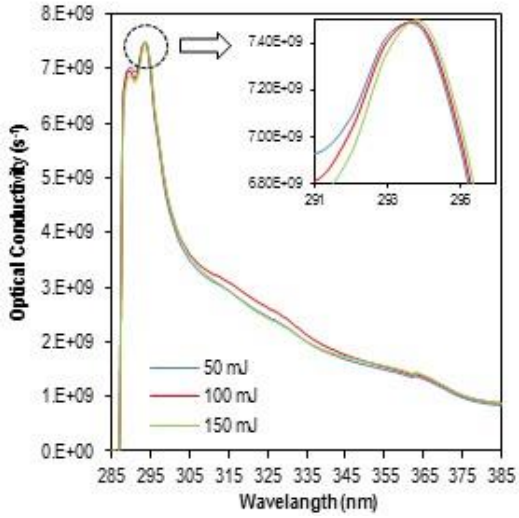

(b)

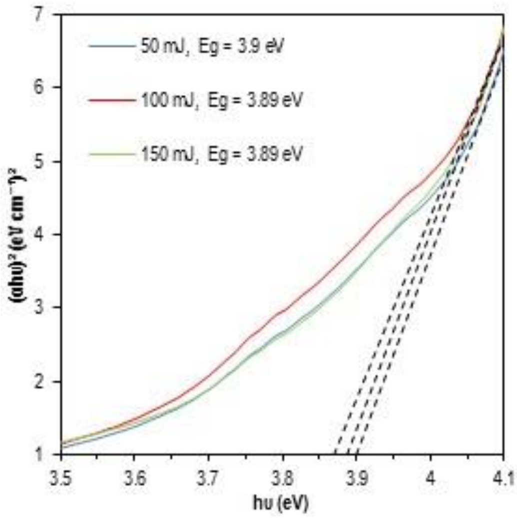

(c)

Fig. (12) UV-visible spectrophotometry analysis of prepared NPs at 1064nm (a) Absorbance, (b) Optical conductivity, and (c) Energy gap

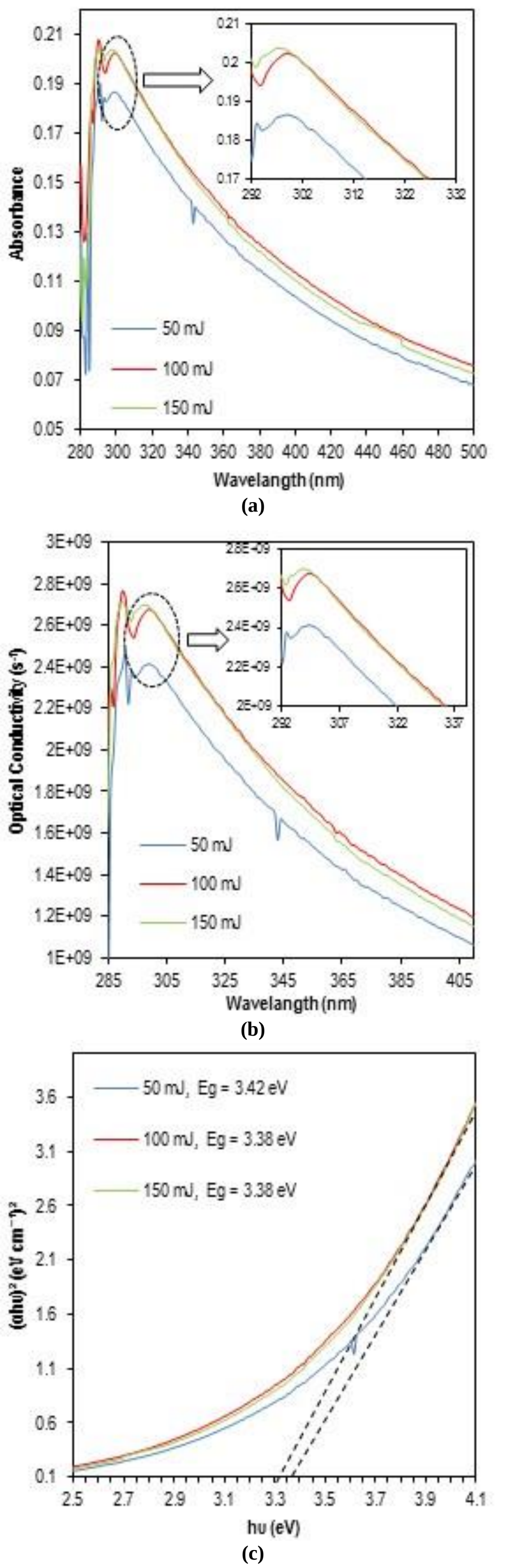

Fig. (13) UV-visible spectrophotometry analysis of prepared NPs at 532nm (a) Absorbance, (b) Optical conductivity, and (c) Energy gap

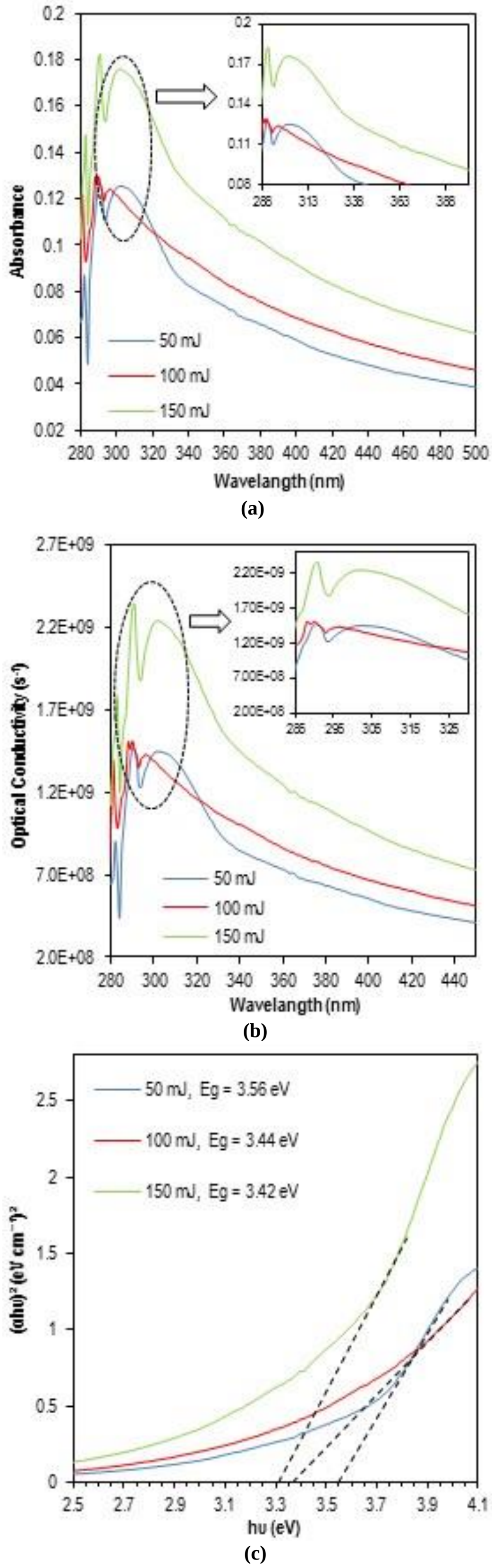

Fig. (14) UV-visible spectrophotometry analysis of prepared NPs at 355nm (a) Absorbance, (b) Optical conductivity, and (c) Energy gap

By analyzing the results of the optical properties, it becomes clear that the optimum wavelength for preparing nickel and nickel oxide NPs within the current working environment is 532nm, which resulted in obtaining smaller average sizes. This was observed in XRD and FE-SEM results.

4. Conclusion

PLAL technique has proven its ability to prepare NPs and its superiority over other techniques in terms of speed, ease, low cost, and the possibility of controlling the physical properties of the prepared NPs by controlling the ablation parameters. It was shown that shorter laser wavelength and higher laser energy used for the preparation of Ni and NiO NPs led to an increase in the oxidation rate and an increase in the concentration of the NPs and thus their aggregation. It was found that the most suitable laser wavelength and energy for the preparation in this study were 532 nm and 150 mJ, meaning that the second harmonic of Nd:YAG laser was the optimum, although the first and third harmonics of the same laser gave good results.

References

[1] K.S. Khashan et al., “Generation of NiO nanoparticles via pulsed laser ablation in deionised water and their antibacterial activity”, *Appl. Phys. A*, 123 (2017) 1-10.
[2] V. Iacono et al., “Pulsed laser ablation production of Ni/NiO nanoelectrocatalysts for oxygen evolution reaction”, *APL Energy*, 1 (2023) 1-8.
[3] K.A. Altammar, “A review on nanoparticles: characteristics, synthesis, applications, and challenges”, *Front. Microbiol.*, 14 (2023) 1-20.
[4] N.A. Hussain, L.Y. Abbas and L.A. Latif, “Preparation of Nickel Oxide Microparticles by Pulsed Laser Ablation and Application to Gas Sensors”, *Eng. Technol. J.*, 39(6) (2021) 1011-1018.
[5] S.N. Rashid et al., “Synthesized Zinc Nanoparticles via Pulsed Laser Ablation: Characterization and Antibacterial Activity”, *Karbala Int. J. Mod. Sci.*, 8(3) (2022) 462-476.
[6] J. Kim et al., “The influence of laser wavelength and fluence on palladium nanoparticles produced by pulsed laser ablation in deionized water”, *Solid State Sci.*, 37 (2014) 96-102.
[7] F. Seifikar et al., “One step synthesis of stable nanofluids of Cu, Ag, Au, Ni, Pd, and Pt in PEG using laser ablation in liquids method and study of their capability in solar-thermal conversion”, *Sol. Ener.*, 246 (2022) 74-88.
[8] K.S. Khashan et al., “Influence of laser energy on the optoelectronic properties of NiO/Si heterojunction”, *J. Phys. Conf. Ser.*, 1795 (2021) 1-6.
[9] M. Safa et al., “Characterizing nickel oxide nanostructures produced by laser ablation method: effects of laser fluence”, *Appl. Phys. A*, 125 (2019) 1-9.
[10] A. Baladi and R. Mamoory, “Effect of Laser Wavelength and Ablation Time on Pulsed Laser Ablation Synthesis of Al Nanoparticles in Ethanol”, *Int. J. Mod. Phys.: Conf. Ser.*, 5 (2012) 58-65.
[11] A.M. Mostafa and E.A. Mwafy, “The effect of laser fluence for enhancing the antibacterial activity of NiO nanoparticles by pulsed laser ablation in liquid media”, *Enviro. Nanotech. Monitor. Manag.*, 14 (2020) 1-8.
[12] H. Huang et al., “Pulsed laser ablation of bulk target and particle products in liquid for nanomaterial fabrication”, *AIP Adv.*, 9 (2019) 1-9.
[13] N.I.S. Yahaya et al., “Synthesis of nickel nanoparticles by pulsed laser ablation in different liquid media”, *Int. Laser Technol. Opt. Symp.*, 2432 (2023) 1-9.
[14] C. Shalichah and A. Khumaeni, “Synthesis of nickel nanoparticles by pulse laser ablation method using Nd: YAG laser”, *IOP J. Phys.: Conf. Ser.*, 1025 (2018) 1-4.
[15] N. Jaji et al., “Advanced nickel nanoparticles technology: From synthesis to applications”, *Nanotech. Rev.*, 9 (2020) 1456-1480.
[16] W. Giurlani, M. Innocenti and A. Lavacchi, “X-ray Microanalysis of Precious Metal Thin Films: Thickness and Composition Determination”, *Coatings*, 8(84) (2018) 1-12.
[17] M.R. Hassani et al., “Synthesis and Applications of Nickel Nanoparticles (NiNPs) - Comprehensive Review”, *J. Ultra Chem.*, 19(1) (2023) 9-37.
[18] J. Wawrzyniak et al., “Laser-Assisted Synthesis and Oxygen Generation of Nickel Nanoparticles”, *Materials*, 13 (2020) 1-13.
[19] M.G. Berhe and Y.T. Gebreslassie, “Biomedical Applications of Biosynthesized Nickel Oxide Nanoparticles”, *Int. J. Nanomed.*, 18 (2023) 4229-4251.
[20] M. Aftab et al., “Effect of Molarity on the Structure, Optical Properties, and Surface Morphology of (002)-Oriented Ni_2O_3 Thin Films Deposited via Spray Pyrolysis”, *Proc. Pakistan Acad. Sci.: A. Phys. Comput. Sci.*, 57(2) (2020) 51-74.
[21] M.K. Khalaf, F.J. Kadhim and O.A. Hammadi, “Fabrication of UV Photodetector from Nickel Oxide Nanoparticles Deposited on Silicon Substrate by Closed-Field Unbalanced Dual Magnetron Sputtering Techniques”, *Opt. Quantum Electron.*, 47(12) (2015) 3805-3813.
[22] A.M. Hameed and M.A. Hameed, “Highly-Pure Nanostructured Metal Oxide Multilayer Structure Prepared by DC Reactive Magnetron Sputtering Technique”, *Iraqi J. Appl. Phys.*, 18(4) (2022) 9-14.
[23] M.A. Hameed, S.H. Faisal, R.H. Turki, “Characterization of Multilayer Highly-Pure Metal Oxide Structures Prepared by DC Reactive Magnetron Sputtering Technique”, *Iraqi J. Appl. Phys.*, 16(4) (2020) 25-30
[24] A.M. Hameed and M.A. Hameed, “Spectroscopic characteristics of highly pure metal oxide nanostructures prepared by DC reactive magnetron sputtering technique”, *Emerg. Mater.*, 6 (2022) 627-633.

[25] L.E. Smart and E.A. Moore, **"Solid State Chemistry: An Introduction"**, 3rd ed., Taylor & Francis, (2005), p. 105.
[26] S.N. Rashid et al., "Evaluation of Laser Influence on Optical Properties of Magnesium Oxide Thin Films Prepared by Drop Casting Method", *Iraqi J. Appl. Phys.*, 19(2) (2023) 33-37.
[27] J. Singh, **"Optical Properties of Materials and Their Applications"**, 2nd ed., John Wiley & Sons Ltd. (2020), p. 69.
[28] K.S. Khashan et al., "Synthesis, characterization and antibacterial activity of colloidal NiO nanoparticles", *Pakistan J. Pharm. Sci.*, 29(2) (2016) 541-546.
[29] S.D. Khairnar and V.S. Shrivastava, "Facile synthesis of nickel oxide nanoparticles for the degradation of Methylene blue and Rhodamine B dye: a comparative study", *J. Taibah Univ. Sci.*, 13(1) (2019) 1108-1118.

Table (1) XRD analysis results of prepared NPs

λ (nm)	NPs	Phase	2θ (deg)	hkl	β (deg)	d (nm)	D (nm)	JCPDS Card No.
1064	NiO	Cubic	37.49	111	0.3	0.239609	27.95335	47-1049
	NiO	Cubic	42.49	200	0.4	0.212498	21.30059	47-1049
	Ni	Cubic	46.73	111	0.2	0.194157	43.25283	00-001-1260
	Ni	Cubic	52.39	002	0.4	0.174434	22.12533	00-001-1260
	NiO	Cubic	63.41	220	0.4	0.146514	23.33545	47-1049
532	NiO	Cubic	38.41	111	0.8	0.234079	10.51148	47-1049
	NiO	Cubic	42.79	200	0.5	0.211077	17.05789	47-1049
	Ni	Cubic	45.25	111	0.3	0.200157	28.67761	00-001-1260
	Ni	Cubic	53.78	002	0.2	0.170249	44.51959	00-001-1260
	NiO	Cubic	62.57	220	0.3	0.148278	30.9745	47-1049
	Ni_2O_3	Hexagonal	66.97	004	0.35	0.139564	27.2042	00-01-0481
355	NiO	Cubic	37.45	111	0.4	0.239856	20.96253	47-1049
	NiO	Cubic	43.39	200	0.15	0.208296	56.9773	47-1049
	Ni	Cubic	44.75	111	0.2	0.202277	42.93874	00-001-1260
	Ni_2O_3	Hexagonal	56.17	202	0.1	0.165099	12.82479	00-01-0481
	NiO	Cubic	62.17	220	0.1	0.148641	15.47332	47-1049

Table (2) EDX analysis results of prepared NPs

λ (nm)	Element	k-ratio	Weight (%)	Atomic (%)
1064	O	48.84	20.65	0.00515
	Ni	51.16	79.35	0.03938
532	O	76.95	47.64	0.00447
	Ni	23.05	52.36	0.00804
355	O	93.56	79.83	0.01501
	Ni	6.44	20.17	0.00481